International Journal of mining and Geo-Engineering

IJMGE

IJMGE 51-2 (2017) 113-118

DOI: 10.22059/ijmge.2017.211646.594615

Predicting the Occurrence of Hydraulic Fracturing in Grouting Operations Based on the Pressure in the Penetrated Cement Grout

Hassan Bakhshandeh Amnieh [a, *], Majid Masoudi [b]

[a] *School of Mining, College of Engineering, University of Tehran, Tehran, Iran*

[b] *Department of Mining Engineering, Faculty of Engineering, University of Kashan, Kashan, Iran*

Article History:

Received: 10 July 2016,

Revised: 24 June 2017,

Accepted: 16 July 2017.

ABSTRACT

Cement grouting is an operation often carried out to consolidate and seal the rock mass in dam sites and tunnels. The quality and efficiency of a grouting operation depends on various factors such as water take, grout properties and grouting pressure. One of the most effective parameters on quality and efficiency is pressure. Application of excessive pressure causes hydraulic fracturing in the rock mass and a low pressure leads to incomplete grouting and failure to seal the site in a perfect manner. In this study, mathematical modeling was used for the first time to predict and determine the optimal pressure. Thus, the joints that existed in the rock mass were simulated using cylindrical shell model. The joints' surroundings were also modeled through the Pasternak environment. To obtain equations governing the joints and the surroundings, the energy method was applied using the Hamilton principle. Finally, an analytical solution method was used to obtain the maximum grouting pressure. In order to validate the modeling, the grouting pressure values obtained by the model were used on the Seymareh and Aghbolagh dams and the relative error rates were measured considering the differences between the calculated and actual pressures. Modeling the examined sections of Seymareh dam showed 29.61, 5.57, 21.98, 32.50 and 9.09 percent error rates and for that of the Aghbolagh dam were 4.32, 5.40 and 2.96 percent. The results indicate that this modeling can be used to estimate the pressure of hydraulic fracturing in grouting operation, and also to prevent its excessive values.

Keywords : *Hydraulic fracturing, Mathematical modeling, Cylindrical shell model, Seymareh and Aghbolagh dams*

1. Introduction

Generally, cement grouting operation is one of the ways to reduce water leakage, increase strength and consolidate jointed rock on the site [1]. In this process, cement grout passes through the grouting section and causes the rock mass to become consolidated and sealed. One of the effective factors on determining the grout penetration distance and increasing operation efficiency is the grouting pressure [2]. By definition, the grouting pressure is the maximum permitted pressure applied at each step of the grouting process by a pump. The range of this pressure usually starts from the minimum required rate for the grout to penetrate into the joints and reaches its maximum permitted value at the end of operation [3]. However, the pressure fluctuates and changes on the hydraulic path between the pumps and the sections, and this point must be taken into account in calculations [4].

There are two main theories regarding the pressure rate: the first is grouting with high pressure in order to increase the influence radius in which the operational expenses are reduced and fewer boreholes are needed [5]. There is also a second theory proposed by other scientists that suggest grouting with low pressure since applying high pressure causes hydraulic fracture in the rock mass and decreases the rock quality [6]. Determining an appropriate range for this parameter has an essential role in the effectiveness of operations [7]. Since a precise criterion or relation has not yet been proposed to determine the suitable pressure, the pressure estimation has always been carried out as an absolutely empirical practice by contractors in workshops [8]. Thus, conducting studies and research projects on this topic is indispensable if one wants to define a certain criterion or scale that contributes to the selection of optimum pressure [9].

After hydrogeological, topographical, geological and geotechnical tests, the grouting pressure is determined for different depths in the ground [10]. The applied pressure is proportionate to the depth of grouting, grout properties, the grouting technique, rock penetrability, jointed rock properties, the status of local stresses, structure dimensions and the physical and mechanical properties of the rock mass. P_g, or pressure at the grouting section is calculated using the relation in (1) [11].

$$P_g = P_{mg} + P_{hg} - P_{hgw} - (f_{cg}+f_{pg}) \quad (1)$$

In this relation, P_{mg} is the grout pressure on barometer at the top of the borehole which is called the grouting manometric pressure in MPa; P_{hg} is the hydrostatic pressure caused by the height of the grout's fluid column in Mpa; P_{hgw}, is the hydrostatic pressure resulted from the height of the underground water column at the grout section in Mpa and f_{pg} and f_{cg} are pressure losses of the grout caused by pipes and fittings in MPa, respectively [12]. The last two values are negligible if obtaining them in shallow boreholes is impossible [13]. However, when multiple connections are used or the length of the borehole is considerable, those values must be calculated based on the physical properties of the pipe such as its diameter and its composing material, as well as the connections properties. The value of P_{mg} can be adjusted and read using a manometer. The values of Pmg and P_{hgw} can be calculated through relations (2) and (3) [14]:

$$P_{hg} = \gamma_g((D_u + Lg/2).\sin\alpha + H_{mg}) \quad (2)$$

$$P_{hgw} = \gamma_w ((D_u + Lg/2).\sin\alpha - D_{gw}) \quad (3)$$

* Corresponding author. Tel.: +(98)-9125230676. *E-mail address:* hbakhshandeh@ut.ac.ir (H. Bakhshandeh).

γ_g is the special weight of the grout. It is the gravitational constant timed the specific gravity and can be stated in form of meganewtons per cubic meter [15]. L is the length of the section in meters and D_u is the distance in meter between the section's upper level in the downward borehole and the point at which excavation started [16]. D_{gw} is the depth of groundwater vertical to the base level in meter, α is the gradient of the borehole, H_{mg} is the vertical distance of the manometer from the groundwater level compared to the base level in meter and γ_w is the special weight of water in meganewtons per cubic meter (Fig. 1) [17].

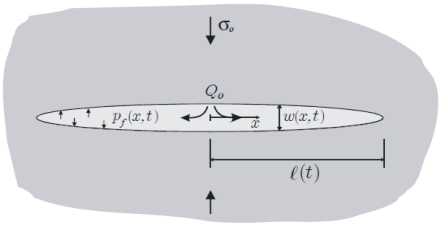

Fig. 1. Grout penetration and hydraulic fracturing in the rock mass [18].

2. Relationship between water take rate in the water pressure test and the amount of grout used in grouting of hydraulically fractured rocks

Water pressure test is used before grouting operation to determine the rate of penetrability, the necessity of grouting and estimations related to it, and the amount of sealing caused by grouting. In this test, the rate of hydraulic conductivity of the rock mass is specified by the penetration of water into the borehole [18]. On some sites, there are rock masses in which the recorded water take in the pressure test is low while the amount of recorded cement grout in the grouting operation is high [19]. However, the joints with low rate of penetration must naturally be inclined to absorb little grout. It is because the hydraulic fracturing phenomenon occurs as a result of too much grouting pressure. Hydraulic fracturing causes joints with little opening to widely open or creates new fractures [20]. Therefore, understanding hydraulic fracturing can be helpful in determining is the reason of difference in the rate of water take and cement grout in these two operations. In the water pressure test, the amount of water that enters the pit under certain pressure is recorded. Absorption of one-liter water per minute for each meter of the borehole at the pressure of one mega Pascal is equal to lugeon [21].

1LU=1lit.min^{-1}.m^{-1}

Lugeon number is always ranges between one and 100 and the value higher than 100 are considered equal to 100:

$$LU=10Q/Pe \tag{4}$$

where Q is the quantity of the water absorbed in liters per meter per minute, P_e is the highest effective pressure in the test and LU is the lugeon value [22].

3. Mathematical modeling

A schematic diagram of a cylindrical shell is shown in Fig. 2 in which geometrical parameters such as length (L), radius (R) and thickness (h) are also indicated. The surrounding foundation is simulated with spring and shear constants.

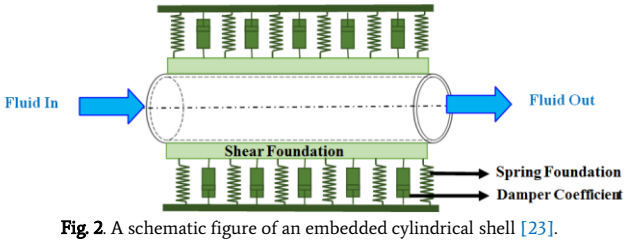

Fig. 2. A schematic figure of an embedded cylindrical shell [23].

3.1. Stress-strain relations

Shear strains γ_{xz} , $\gamma_{\theta z}$ are considered negligible in the Kirchhoff deformation theory. Hence, the tangential displacements u and v become the linear functions of the radial coordinate (z) [23]. In other words,

$$\begin{aligned} u(x,\theta,z) &= u(x,\theta) - z\frac{\partial w(x,\theta)}{\partial x},\\ v(x,\theta,z) &= v(x,\theta) - z\frac{\partial w(x,\theta)}{\partial \theta},\\ w(x,\theta,z) &= w(x,\theta). \end{aligned} \tag{5}$$

The strain components $\bar{\varepsilon}_{xx}$, $\bar{\varepsilon}_{\theta\theta}$ and $\bar{\gamma}_{x\theta}$ at an arbitrary point of the shell are related to the middle surface strains ε_{xx}, $\varepsilon_{\theta\theta}$ and $\gamma_{x\theta}$ and to the changes in the curvature and torsion of the middle surface k_{xx}, $k_{\theta\theta}$ and $k_{x\theta}$ by the following relationships:

$$\begin{Bmatrix} \bar{\varepsilon}_{xx} \\ \bar{\varepsilon}_{\theta\theta} \\ 2\bar{\varepsilon}_{x\theta} \end{Bmatrix} = \begin{Bmatrix} \varepsilon_{xx} \\ \varepsilon_{\theta\theta} \\ \gamma_{x\theta} \end{Bmatrix} - z\begin{Bmatrix} k_{xx} \\ k_{\theta\theta} \\ k_{x\theta} \end{Bmatrix} = \left(\begin{bmatrix} \frac{\partial}{\partial x} & 0 & 0 \\ 0 & \frac{\partial}{R\partial\theta} & \frac{1}{R} \\ \frac{\partial}{2R\partial\theta} & \frac{\partial}{2\partial x} & 0 \end{bmatrix} - z\begin{bmatrix} 0 & 0 & \frac{\partial^2}{\partial x^2} \\ 0 & 0 & \frac{\partial^2}{R^2\partial\theta^2} \\ 0 & 0 & 2\frac{\partial^2 w}{R\partial x\partial\theta} \end{bmatrix} \right) \times \begin{bmatrix} u \\ v \\ w \end{bmatrix}, \tag{6}$$

Where u, v and w, describe the displacements in the orthogonal coordinate system x, θ, z established at the middle surface of the shell.

Using Hook law, the constitutive equation may be expressed as follows (Ghorbanpour Arani, 2011a, 2011b):

$$\begin{Bmatrix} \sigma_{xx} \\ \sigma_{\theta\theta} \\ \sigma_{x\theta} \end{Bmatrix} = \begin{bmatrix} C_{11} & C_{12} & 0 \\ C_{12} & C_{22} & 0 \\ 0 & 0 & C_{66} \end{bmatrix} \left[\begin{Bmatrix} \frac{\partial u}{\partial x} \\ \frac{\partial v}{R\partial\theta} + \frac{w}{R} \\ \frac{\partial u}{R\partial\theta} + \frac{\partial v}{\partial x} \end{Bmatrix} - z\begin{Bmatrix} \frac{\partial^2 w}{\partial x^2} \\ \frac{\partial^2 w}{R^2\partial\theta^2} \\ 2\frac{\partial^2 w}{R\partial x\partial\theta} \end{Bmatrix} \right], \tag{7}$$

Where σ_{ij} (i, j = x, θ) stresses as well as u, v, w are the displacements of an arbitrary point of the shell in axial, circumferential and radial directions, respectively. Also, C_{ij}, i, j=1,...,6) correspond to elastic constants [23].

3.2. Energy method

The total potential energy of the pipe is the sum of strain energy, kinetic energy and work conducted by flowing fluid. The strain energy is [23]:

$$U = \int_{-\frac{h}{2}}^{\frac{h}{2}} \iint_A \left(\sigma_{xx}\left(\frac{\partial u}{\partial x} - z\frac{\partial^2 w}{\partial x^2} \right) + \sigma_{\theta\theta}\left(\frac{\partial v}{R\partial\theta} + \frac{w}{R} + -z\frac{\partial^2 w}{R^2\partial\theta^2} \right) + \sigma_{x\theta}\left(\frac{\partial u}{R\partial\theta} + \frac{\partial v}{\partial x} - 2z\frac{\partial^2 w}{R\partial\theta\partial x} \right) \right) dz\, dA, \tag{8}$$

and the kinetic energy is:

$$K = \frac{\rho}{2}\int_v \left((\frac{\partial u}{\partial t})^2 + (\frac{\partial v}{\partial t})^2 + (\frac{\partial w}{\partial t})^2 \right) dV, \tag{9}$$

and the work conducted by internal viscose fluid is (Wang and Ni, 2009):

$$W = \int (F_{fluid}) w dA = \int \left(-h\rho_f \left(\frac{\partial^2 w}{\partial t^2} + 2v_x\frac{\partial^2 w}{\partial x\partial t} + {v_x}^2\frac{\partial^2 w}{\partial x^2} \right) + h\mu\left(\frac{\partial^3 w}{\partial x^2\partial t} + \frac{\partial^3 w}{R^2\partial\theta^2\partial t} + v_x\left(\frac{\partial^3 w}{\partial x^3} + \frac{\partial^3 w}{R^2\partial\theta^2\partial x} \right) \right) \right) w dA \tag{10}$$

Now, by replacing these terms in the following expression, based on Hamilton principal:

$$\int_0^t (\delta K - \delta U + \delta W) dt = 0, \tag{11}$$

and defining the following non-dimensional quantities:

$$\{\bar{u},\bar{v},\bar{w}\}=\frac{\{u,v,w\}}{h},\quad \gamma=\frac{h}{l},\quad \xi=\frac{x}{l},\quad \beta=\frac{h}{R},\quad \bar{C}_{ij}=\frac{C_{ij}}{C_{11}},$$
$$\bar{\rho}=\frac{\rho_s}{\rho_f},\quad \mu=\frac{\mu_0}{h\sqrt{C_{11}\rho_f}},\quad V=v_x\sqrt{\frac{\rho_f}{C_{11}}},\quad \bar{t}=\frac{t}{h\sqrt{\frac{\rho_f}{C_{11}}}},\tag{12}$$

the four electro-thermo mechanical coupling governing equations of PVDF cylindrical shell conveying viscose fluid, can therefore be written as [24]:

$$\gamma^2\left(\frac{\partial^2\bar{u}}{\partial\xi^2}+\frac{\partial\bar{w}}{\partial\xi}\frac{\partial^2\bar{w}}{\partial\xi^2}\right)+\gamma\beta\bar{C}_{12}\left(\frac{\partial^2\bar{v}}{\partial\xi\partial\theta}+\frac{\partial\bar{w}}{\partial\xi}+\beta_s\frac{\partial\bar{w}}{\partial\theta}\frac{\partial^2\bar{w}}{\partial\xi\partial\theta}\right)+\beta\bar{C}_{66}\left(\beta\frac{\partial^2\bar{u}}{\partial\theta^2}+\frac{\partial^2\bar{v}}{\partial\xi\partial\theta}\right.$$
$$\left.+\beta\frac{\partial\bar{w}}{\partial\xi}\frac{\partial^2\bar{w}}{\partial\theta^2}+\frac{\partial\bar{w}}{\partial\xi}+\beta\frac{\partial\bar{w}}{\partial\theta}\frac{\partial^2\bar{w}}{\partial\xi\partial\theta}\right)+\gamma^2\bar{e}_{11}\frac{\partial^2\Phi}{\partial\xi^2}=(\bar{\rho})\frac{\partial^2\bar{u}}{\partial\bar{t}^2},\tag{13}$$

$$\beta\bar{C}_{12}\left(\frac{\partial^2\bar{u}}{\partial\xi\partial\theta}+\frac{\partial\bar{w}}{\partial\xi}\frac{\partial^2\bar{w}}{\partial\xi\partial\theta}\right)+\beta^2\bar{C}_{22}\left(\frac{\partial^2\bar{v}}{\partial\theta^2}+\frac{\partial\bar{w}}{\partial\theta}+\beta\frac{\partial\bar{w}}{\partial\theta}\frac{\partial^2\bar{w}}{\partial\theta^2}\right)+\gamma\bar{C}_{66}\left(\frac{\beta\partial^2\bar{u}}{\partial\xi\partial\theta}+\frac{\partial^2\bar{v}}{\partial\xi^2}\right.$$
$$\left.+\frac{\beta\partial^2\bar{w}}{\partial\theta\partial\xi}\frac{\partial\bar{w}}{\partial\xi}+\frac{\beta\partial\bar{w}}{\partial\theta}\frac{\partial^2\bar{w}}{\partial\xi^2}\right)+\beta\bar{e}_{12}\frac{\partial^2\Phi}{\partial\xi\partial\theta}=\bar{\rho}\frac{\partial^2\bar{v}}{\partial\bar{t}^2},\tag{14}$$

$$\frac{\gamma^2}{12}\left(-\gamma^2\frac{\partial^4\bar{w}}{\partial\xi^4}-\bar{C}_{12}\beta^2\frac{\partial^4\bar{w}}{\partial\xi^2\partial\theta^2}\right)+\frac{1}{12}\left(-\gamma^2\beta^2\bar{C}_{12}\frac{\partial^4\bar{w}}{\partial\xi^2\partial\theta^2}-\beta^4\bar{C}_{22}\frac{\partial^4\bar{w}}{\partial\theta^4}\right)$$
$$-\frac{\gamma\beta\bar{C}_{12}}{3}\left(\frac{\partial\bar{u}}{\partial\xi}+\frac{\gamma}{2}\left(\frac{\partial\bar{w}}{\partial\xi}\right)^2\right)-\beta\bar{C}_{22}\left(\frac{\partial\bar{v}}{\partial\theta}+\beta\bar{w}+\frac{\beta^2}{2}\left(\frac{\partial\bar{w}}{\partial\theta}\right)^2\right)-$$
$$-\left[\frac{\partial^2\bar{w}}{\partial\bar{t}^2}+2\gamma V\frac{\partial^2\bar{w}}{\partial\xi\partial\bar{t}}+\gamma^2V^2\frac{\partial^2\bar{w}}{\partial\xi^2}\right]$$
$$-\mu\left[\gamma^2\frac{\partial^3\bar{w}}{\partial\xi^2\partial\bar{t}}+V\gamma^3\frac{\partial^3\bar{w}}{\partial\xi^3}+\beta^2\left(\frac{\partial^3\bar{w}}{\partial\theta^2\partial\bar{t}}+V\gamma\frac{\partial^3\bar{w}}{\partial\theta^2\partial\xi}\right)\right]+\gamma\beta\bar{e}_{12}\frac{\partial\Phi}{\partial\xi}=\bar{\rho}\frac{\partial^2\bar{w}}{\partial\bar{t}^2},\tag{15}$$

4. Navier method

Simply considering the supported boundary condition, the mechanical displacement may be written as [24]:

$$w(x,\theta)=w_0\sin(\frac{n\pi x}{L})\sin(m\theta),\tag{16}$$

$$u(x,\theta)=u_0\cos(\frac{n\pi x}{L})\sin(m\theta),\tag{17}$$

$$v(x,\theta)=v_0\sin(\frac{n\pi x}{L})\cos(m\theta),\tag{18}$$

Substituting Eq. (12) into Eqs. (9) - (11) results in:

$$\begin{bmatrix}K_{11}&K_{12}&K_{13}\\K_{21}&K_{22}&K_{23}\\K_{31}&K_{32}&K_{33}\end{bmatrix}\begin{bmatrix}u_0\\v_0\\w_0\end{bmatrix}=0,\tag{19}$$

The displacement may be obtained by solving the equation above. Using the obtained displacement and Eq. (10), the fluid pressure can be calculated [24].

5. Modeling Details

The parameters shown in Table 1 were inserted into the mathematical model as the input data.

6. Case study

6.1. Seymareh dam

Seymareh dam and its power plant are located 40 km northwest of Dareshahr city and 7.5 km from Cheshme Shirin village in Ilam province, Iran. Its purpose is to use the potential power in Seymareh River. Seymareh is a thin double-arched concrete dam with the height of 130m from the current river bed (and about 180m from the bedrock). The dam crest elevation is 730 m, and at the normal elevation, the water height is 720 m above the sea level. The length of the dam crest at its elevated part is 202 m. The capacity of the dam reservoir is 3.215 billion cubic meters.

Table 1. Model input data.

Row	Name of the input parameter	Value of the input parameter
1	Dimensions of the given rock	1*1
2	Density of the rock	2.7 grams per cubic centimeter
3	Joint aperture (b)	1 mm
4	Elasticity module	1130 kg/m^3
5	Shear stiffness coefficient	10^9
6	Poisson's ratio	0.3
7	Grout penetration range	46.5 cm
8	Borehole radius	3.5 cm

First of all, in order to examine the rate of rock penetrability, the water pressure test was carried out on boreholes. Then, when the rate of hydraulic conduction in the rock environment was specified, the cement grouting operation was performed to seal the base and support of the dam. In Table 2, some results of water take and cement grout in boreholes P-19, P-20, P-22 and P-23 are shown. According to these data, it can be seen that in borehole P-19 in sections 3 and 4, in borehole P-20 in section 6, in borehole P-22 in section 4 and in borehole P-23 in section 11, the rate of water takes obtained by lugeon number is low while the cement grout take is high. Generally, this difference in water take and cement take processes indicates the occurrence of hydraulic fracturing phenomenon due to the excessive pressure in the cement grouting procedure.

6.2. Aghbolagh dam

Aghbolagh earth dam is located 32 km in south of the Borujen City in Chahar Mahal-o-Bakhtiari province in Iran. The geographical coordinates of the dam axis in the UTM system are x=520363 and y=3512353. Considering the geological map, the area of interest is located in the Zagros mountain range under the over-thrust zone.

From a stratigraphic perspective, the Mesozoic, Cenozoic and particularly the Cretaceous rocks are dominant in this zone, and from a structural point of view, large faults such as the main Zagros fault and Dena fault play major roles in the zone.

In this site, pilot grouting operation was conducted in the limestone units on the right side of the dam as the most important part of the whole grouting process with respect to sealing. The arrangement of TG-1, TG-2 and TG-3 grouting boreholes is in such a form that they are placed on the vertices of an equilateral triangle each side of which is three meters long. In each borehole, lugeon experiments are conducted first. After obtaining the results, plans for the mixture of water, cement and other additives are selected. Grouting operation is carried out in five-meter-long sections and the results are shown in Table 3.

According to the results shown in Table 3, we can see that in the depths of 25-30 and 30-35 meters in borehole TG-1, the rate of water take is low (LU=2) while the amount of the grouted cement is high. The values of aforementioned variables are 1175 and 1325, respectively. In the depth of 32-45 meters in borehole TG-2, the water take was also low (LU=2) but the cement take was very high and equaled 2466 kg. The difference between low water absorption compared to high grout take indicates excessive increase in the cement grout's penetration pressure and occurrence of hydraulic fractures in the grouting process.

7. Results of modeling

In this section, based on the results obtained from the water pressure test and grouting operation on the Seymareh and Aghbolagh dams and comparing the real pressure values with the calculated pressure acquired through modeling, the results achieved by modeling were validated. The resulting information consists of pressure values in the boreholes where water take in the water pressure test is low while grout take in the grouting operation is high. This shows that hydraulic fracturing has occurred in these sections. These data are shown in Table 4. In Fig. 3, the

degree of convergence among these values is shown.

Table 2. Results of water pressure test and grouting in some boreholes of the Seymareh dam.

Data obtained from P-22 borehole				
Number of section	Depth(m)	LU	P(pa)	V(m3)
1	0-5	11.4	233000	0.021625
2	5-10	41.5	376000	0.032417
3	10-15	20.5	523000	0.068458
4	15-20	39.4	764000	7.291667
5	20-25	<1	964000	0.154208
6	25-30	3.1	1162000	0.106833
7	30-35	7	1299000	0.097375
8	35-40	<1	1587000	0.005375
9	40-45	<1	1794000	0.010792
10	45-50	6.4	2230000	0.022167
11	50-53	18.5	2082000	0.256125

Data obtained from P-19 borehole				
Number of section	Depth(m)	LU	P(pa)	V(m3)
1	0-5	54.3	130000	0.012667
2	5-10	29.8	377000	0.012667
3	10-15	10.9	521000	5.291667
4	15-20	6.7	695000	8.691667
5	20-25	11.54	1015000	0.006333
6	25-30	26.9	1066000	0.012667
7	30-35	2.2	1291000	0.038
8	35-40	4.5	1682000	0.022167
9	40-45	<1	1743000	0.022167
10	45-50	3.6	3980000	0.019
11	50-53	11.2	2381000	0.025325

Data obtained from P-20 borehole				
Number of section	Depth(m)	LU	P(pa)	V(m3)
1	0-5	3.8	230000	0.012667
2	5-10	2.7	377000	0.012667
3	10-15	22.4	523000	0.0095
4	15-20	69.9	552000	5.216667
5	20-25	<1	974000	0.015833
6	25-30	22.8	1029000	7.654167
7	30-35	1.34	1247000	0.025333
8	35-40	<1	1456000	0.022167
9	40-45	<1	1639000	0.019
10	45-50	<1	2064000	0.015833
11	50-53	19.54	1886000	2.6665

Data obtained from P-23 borehole				
Number of section	Depth(m)	LU	P(pa)	V(m3)
1	0-5	51.3	225000	0.172625
2	5-10	72.2	343000	0.123333
3	10-15	10.3	522000	0.026667
4	15-20	5	767000	0.019458
5	20-25	4.1	795000	0.049417
6	25-30	95	1037000	3.110833
7	30-35	6.1	1207000	0.074667
8	35-40	1.82	1445000	0.127667
9	40-45	<1	1663000	0.004833
10	45-50	3.8	2074000	0.021083
11	50-53	18.2	2232000	3.98665

Table 3. Results of the water pressure test and grouting in some boreholes of the Aghbolagh dam.

Borehole name	Depth	LU	Cement take (kg)
TG-1	4-6	100	134
	6-10	100	242
	10-15	14	151
	15-20	25	536
	20-25	1	114
	25-30	2	1175
	30-35	2	1325
	35-40	1	627
	40-45	26	3335
TG-2	4-7/3	100	573
	7/3-12	12	486
	12-17	49	133
	17-22	100	1971
	22-27	1	44
	27-32	1	38
	32-45	2	2466
TG-3	4/2-5/8	100	462
	5/8-8/3	100	201
	8/3-13	37	104
	18-23	1	38
	23-28	1	33
	28-33	1	no injection
	33-38	1	no injection
	38-43	1	no injection
	43-45	1	no injection

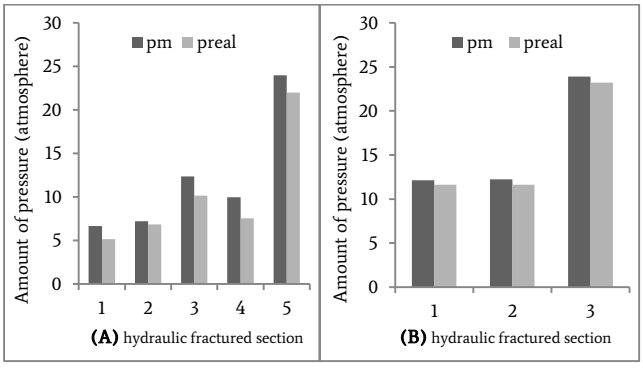

Fig. 3. Convergence rate between measured fracturing pressure (P_m) and real fracturing pressure (P_{real}) in grouting operations in A) Seymareh and B) Aghbolagh dams.

8. Comparison and analysis of the results

According to the results shown in Fig. 2, it can be seen that there is a high degree of convergence between the values of the real recorded pressure in Seymareh dam-construction workshops and the values measured through modeling. In order to validate the modeling, relative error of the measured pressure (P_m) was compared to the real recorded pressure (P_{real}) obtained from $E= [(P_{real}-P_m)/P_{real}]*100$. The results are shown in Table 4.

Table 4. Comparison between grout pressures that result in hydraulic fracturing in grouting operations and the calculated fracturing pressure in atmosphere and the relative error values.

Aghbolagh dam					
Name of the borehole	**Section depth (m)**	**Penetrating grout velocity (cm/s)**	**Calculated pressure**	**Recorded pressure**	**relative error values**
TG-1	25-30	V=5985	12.1123	11.61	4.32
TG-1	30-35	V=7469	12.2379	11.61	5.40
TG-2	32-45	V=8231	23.9081	23.22	2.96
Seymareh dam					
Name of the borehole	**Section depth (m)**	**Penetrating grout velocity (cm/s)**	**Calculated pressure**	**Recorded pressure**	**relative error values**
p-19	10-15	V=11108	6.6623	5.14	29.61
p-19	15-20	V=29683	7.2319	6.85	5.57
p-20	25-30	V=7678	12.3819	10.15	21.98
p-22	15-20	V=4234	9.9910	7.54	32.50
p-23	50-53	V=8341	24.0012	22	9.09

The results shown in Tables 2 and 4 indicate that there is a desirable correlation between calculated fracturing pressure and the fracturing pressure recorded in the Seymareh and Aghbolagh dam-construction

sites. This shows that the proposed model has the desirable precision in predicting and estimating the rate of hydraulic fracturing.

9. Sensitivity analyses

In this section, sensitivity analyses were conducted to understand the effect of model parameters on the response. For this purpose, the statistical analysis by SPSS software was also used. In this analysis, the most important parameters for estimation of the grout pressure that are obtained from cores and grouting boreholes in dam-sites include the joint aperture (b), density of the rock (d), shear stiffness coefficient (scc), elasticity module (E), Poisson's ratio (pc). SPSS software was used in this section to analyze the relationship between the dependent parameter (P) and the independent variables and to determine the effects of independent parameters in estimation of grouting pressure. This analysis was used based on the data obtained from grouting sites. A sample of the output data from the software was illustrated in Tables 5 and 6.

Table 5. The results in SPSS output: the multiple correlation coefficient R and the square of the multiple correlation coefficient R^2 and Adjusted R Square and std. Error of the Estimate.

Model	R	R Square	Adjusted R Square	Std Error of the Estimate
1	0.981	0.962	0.954	1.45470

According to the square of the multiple correlation coefficient (R^2) in Table 5 it can be seen that there is a high correlation between the dependent and the independent variables, so that this determination coefficient (R^2) is 0.962.

Table 6. SPSS output considering the sum of input data: correlation coefficients, Constant value, unstandardized coefficients for the independent variables (B), standard error (Std.Error), Beta standardized coefficients, t-test and level of significance (sig).

Model	Unstandardized Coefficients		Standardized Coefficients	t	Sig.
	B	Std Error	Beta		
1 (Constant)	5.2	0.070		-2.102	0.089
b	0.7	0.001	0.001	-0.473	0.656
d	0.5	0.001	1.00	1258.463	0.00
scc	0.25	0.000	0.001	0.894	0.412
E	0.13	0.002	0.00	0.726	0.500
pc	0.09	0.001	0.001	1.835	0.126

In Table 6, column B, unstandardized coefficients for the independent variables shows the effectiveness of the parameters to estimate the grouting pressure. It can be seen that the most effective parameters are joint aperture (b), density of the rock (d), shear stiffness coefficient (scc), elasticity module (E) and Poisson's ratio (pc), respectively.

10. Conclusion

The required rate of grouting pressure to prevent the hydraulic fracturing phenomenon was examined in this study. Not only the occurrence of hydraulic fracturing practically prevents achieving the goals of grouting, namely sealing and improving the site, but it also causes most of the joints to open, creates fractures in the rock mass, and deteriorates its quality. Therefore, it is highly important to estimate the rate of grouting pressure which causes fracturing. To do so, mathematical modeling and simulation of the joint conditions were conducted using a cylindrical shell and the fracturing pressure was calculated. In order to validate the results, real values of hydraulic fracturing pressure recorded in grouting operations in the Seymareh and Aghbolagh dams were used and the processes of change in real pressure values and calculated pressure values were controlled. The results showed that there were desirable convergence and correlation between these two sets of values. In addition, calculation of the relative error between the values showed that the mathematical model in the sections of the Seymareh dam had the error values of 29.61, 5.57, 21.98, 32.50 and 9.09 percent and in the Aghbolagh dam sections, the error values were to be 4.32, 5.40 and 2.96 percent. These results indicate that mathematical modeling can be used to predict the occurrence of hydraulic fracturing phenomenon in grouting operations and thus increase the efficiency and productivity of such processes. In order to understand the effect of model parameters on the response, sensitivity analysis by SPSS software was conducted. Results showed that the most effective parameters are joint aperture (b), density of the rock (d), shear stiffness coefficient (scc), elasticity module (E) and Poisson's ratio (pc) respectively.

REFRENCES

[1] Economides, M. J. (1990). 1 Implications of Cementing on Well Performance. Developments in Petroleum Science, 28, 1-1.

[2] Wong, H. Y., & Farmer, I. W. (1973). Hydrofracture mechanisms in rock during pressure grouting. Rock mechanics, 5(1), 21-41.

[3] Rice, J. R. (1968). Mathematical analysis in the mechanics of fracture. Fracture: an advanced treatise, 2, 191-311.

[4] Garagash, D. I. (2003). Evolution of a plane-strain fracture driven by a power-law fluid. In Electronic Proc. 16th ASCE Eng. Mech. Conf., July 16–18 (pp. 219-234).

[5] Van Dam, D. B. (1999). The influence of inelastic rock behaviour on hydraulic fracture geometry. TU Delft, Delft University of Technology.

[6] Cleary, M. P., Johnson, D. E., Kogsbøll, H. H., Owens, K. A., Perry, K. F., De Pater, C. J., & Mauro, T. (1993, January). Field implementation of proppant slugs to avoid premature screen-out of hydraulic fractures with adequate proppant concentration. In Low permeability reservoirs symposium. Society of Petroleum Engineers.

[7] Van Dam, D. B. (1999). The influence of inelastic rock behaviour on hydraulic fracture geometry. TU Delft, Delft University of Technology.

[8] van de Ketterij, R. G. (2001). Optimisation of the near-wellbore geometry of hydraulic fractures propagating from cased perforated completions. TU Delft, Delft University of Technology.

[9] Weijers, L. (1995). The near-wellbore geometry of hydraulic fractures initiated from horizontal and deviated wells (Doctoral dissertation, TU Delft, Delft University of Technology).

[10] Sneddon, I. N., & Transforms, F. (1951). McGraw Hill Book Co. Inc., New York.

[11] Lhomme, T. P. Y. (2005). Initiation of hydraulic fractures in natural sandstones. TU Delft, Delft University of Technology.

[12] Fett, T. (1999). Estimated stress intensity factors for semi-elliptical cracks in front of narrow circular notches. Engineering Fracture Mechanics, 64(3), 357-362.

[13] Creager, M., & Paris, P. C. (1997). Elastic field equations for blunt cracks with reference to stress corrosion cracking. International Journal of Fracture Mechanics, 3(4), 247-252.

[14] Yew, C. H., & Weng, X. (2014). Mechanics of hydraulic fracturing. Gulf Professional Publishing.

[15] Mack, M. G., & Elbel, J. L. (1994). A Simulator for Modeling Acid Fracturing Treatments. In Proc.

[16] Gulrajani, S. N., Nolte, K. G., & Romero, J. (1997, January). Evaluation of the M-Site B-sand fracture experiments: The evolution of a pressure analysis methodology. In SPE Annual Technical Conference and Exhibition. Society of Petroleum Engineers.

[17] Vinegar, H. J., Wills, P. B., DeMartini, D. C., Shlyapobersky, J., Deeg, W. F. J., Adair, R. G., & Sorrells, G. G. (1992). Active and passive seismic imaging of a hydraulic fracture in diatomite. Journal of

Petroleum Technology, 44(01), 28-90.

[18] Johnson, E., & Cleary, M. P. (1991, January). Implications of recent laboratory experimental results for hydraulic fractures. In Low Permeability Reservoirs Symposium. Society of Petroleum Engineers.

[19] Tolppanen, P., & Syrjänen, P. (2003). Hard rock tunnel grouting practice in Finland. Sweden, and Norway–Literature Study by Finnish Tunnelling Association.

[20] Shroff, A. V., & Shah, D. L. (1999). Grouting technology in tunnelling and dam construction. A. A. Balkema. 626, 626.

[21] El Tani, M. (2012). Grouting rock fractures with cement grout. Rock mechanics and rock engineering, 45(4), 547-561.

[22] Houlsby, A. C. (1990). Construction and design of cement grouting: a guide to grouting in rock foundations (Vol. 67). John Wiley & Sons.

[23] Arani, A. G., Kolahchi, R., & Barzoki, A. M. (2011). Effect of material in-homogeneity on electro-thermo-mechanical behaviors of functionally graded piezoelectric rotating shaft. Applied Mathematical Modelling, 35(6), 2771-2789.

[24] Wang, L., & Ni, Q. (2009). A reappraisal of the computational modelling of carbon nanotubes conveying viscous fluid. Mechanics Research Communications, 36(7), 833-837.